
Article:
Pope, J.J., Calvert, E.L., Weston, N.S. orcid.org/0000-0002-0515-4573 et al. (1 more author) (2019) FAST-DB: A novel solid-state approach for diffusion bonding dissimilar titanium alloy powders for next generation critical components. Journal of Materials Processing Technology, 269. pp. 200-207. ISSN 0924-0136

https://doi.org/10.1016/j.jmatprotec.2019.02.011

---

1. Introduction

Titanium alloys have a high strength to weight ratio, excellent corrosion resistance and fatigue performance, and are used predominantly in the aerospace sector and chemical plant industry, as summarised by (Lütjering and Williams, 2007).

Titanium aerospace components, such as disks and blades are normally machined from a near net shape titanium alloy forging or bar stock, respectively. Such components are subjected to a range of thermal and mechanical stresses in service. A compressor blade for example, requires high creep performance in the aerofoil and high fatigue properties in the root section. When a component is processed using a single alloy, the performance can be compromised in high stress regions and over engineered in less demanding regions. However, if dissimilar alloys are used in the same component, subcomponent features and sections could be tailored for specific local properties under specific stress states. Such a processing capability will provide designers and engineers with much greater freedom for demanding applications.

Field assisted sintering technology (FAST) is an emerging process for consolidating metallic powders, and has recently been identified as a processing method for diffusion bonding titanium alloy powders. It has several advantages over powder consolidation processes such as hot isostatic pressing (HIP). (Suárez et al., 2013) demonstrated it is approximately 3-4 times faster than HIP, due to high and efficient heating rates achieved by a unique Joule heating effect, in addition to homogeneous heating throughout cylindrical samples. Furthermore, the mandatory HIP canning process which includes degassing and welding of the mild steel can, and then post HIP removal, is not required for FAST. Instead, shaped reusable graphite moulds are

used, reducing processing costs and making FAST a cost-effective process. From a joining standpoint, FAST is also a solid-state processing method that has no macroscopic chemical segregation or gas porosity issues, like those associated with fusion welding. Solid-state bonding processes such as friction stir welding (FSW), diffusion bonding, and linear friction welding (LFW) have previously been used to join dissimilar titanium alloys.

(Gangwar et al., 2016) demonstrated FSW to be an effective method of joining alpha-beta titanium alloys ATI-425 and TIMET-54M. The authors found the material selection for the advancing or retreating sides influenced the mixing patterns, however the microstructure located in the weld nugget region was similar, regardless of which material was on the advancing side. (Gudipati and Kosaka, 2016) diffusion bonded alpha-beta TIMET alloy 54M with Ti-6-4 and Ti-6Al-2Sn-4Zr-2Mo-0.1Si (Ti-6242S). 54M showed superior diffusion bonding properties due to the lower flow stress at a certain temperature and strain rate compared to the other alloys, increasing the surface area at the bonding interface. (Ji et al., 2016) used linear friction welding (LFW) to join Ti-6Al-4V with Ti-5Al-2Sn-2Zr-4Mo-4Cr, where the authors found a high hardness region in the weld zone, believed to be attributed to fine recrystallised grains [4]. Tensile tests showed failure occurred in the Ti-6-4 alloy, 1.2 mm away from the friction weld interface.

Previous research into joining metallics using FAST has mostly concentrated on bonding fully consolidated billets and sheets together, while bonding dissimilar powders has been limited. Titanium powder and titanium sheets have been joined to dissimilar materials using the FAST process, or even as a filler material to reduce the residual stresses between two materials. (Pripanapong et al., 2016) diffusion bonded CP-Ti rod and various cast Mg alloy rods using FAST, and showed bond tensile strengths of up to 96.3% of the Mg alloy strength. Sheet Ti-6Al-4V and AISI 4330

steel dissimilar metals have been bonded by (Miriyev et al., 2013) using FAST, where at the interface a titanium carbide layer was formed, which prevented the formation of brittle intermetallics between the two alloys. (Vicente et al., 2013) diffusion bonded CP-Ti with cobalt alloy powder Co-28Cr-6Mo, presintered CP-Ti with cobalt alloy powder, and presintered cobalt alloy powder with CP-Ti powder, using FAST. They found that the hardness difference of the alloys had an effect on whether a straight or irregular interface was formed. (Chen et al., 2015) reported that titanium can be successfully used as an interlayer between pure dissimilar metals of W and Fe, in both powder and foil form, to reduce residual stresses produced by the different thermal expansion coefficients.

From a similar material perspective, (He et al., 2012) showed that bonding Ti-6-4 plates using FAST yields high tensile strengths of 91.4% of the bulk material, using a low dwell temperature of only 700°C. These bond strengths were higher compared to those produced through a traditional hot-pressing processing route.

A range of titanium powder chemistries and morphologies have been consolidated using FAST. (Weston et al., 2015) demonstrated the flexibility of FAST by consolidating different feedstocks and achieved densities of up to 99.9% by optimising the FAST parameters. (Zhao et al., 2016) bonded Ti-45Al-7Nb-0.3W prealloyed powder using FAST, prior to being processed by HIP where the bonding strength exceeded the bulk material strength. (Shahedi et al., 2018) processed CP-Ti using FAST at temperatures between 750 and 1350°C, and found the optimal temperature to be 1200°C, whereby the lowest porosity and best mechanical properties were observed. (Calvert et al., 2018) showed that metastable beta alloy Ti-5553 can be consolidated using FAST to high densities. A subsequent small-scale

upsetting and heat treatment of the FAST samples showed the flow stress behaviour and microstructures are similar to that of a conventional processing route.

Recently, FAST has been demonstrated as a method of joining different materials by producing a composite from aluminium AA2024 powder infiltrated with TiNi fibres by (Dong et al., 2016). The FAST process has also been exploited by (Martin et al., 2016) to produce architectured microstructures in titanium alloys by combining electron beam melting (EBM) with FAST. This consisted of an EBM lattice structure filled by a powder titanium alloy, and achieved densities greater than 99%.

In this study, the authors have undertaken experiments using FAST to diffusion bond dissimilar titanium alloy powders: specifically commercially pure Ti (CP-Ti) grade 2 alpha alloy; the most widely used alpha-beta type alloy Ti-6Al-4V; and a metastable beta type alloy Ti-5Al-5Mo-5V-3Cr (Ti-5553) which is used for high strength aerospace forging applications, highlighted by (Boyer and Briggs, 2005). This unique bonding process has been termed “FAST-DB” for titanium alloys, and is schematically illustrated in Fig. 1. The process starts with a layup of powders which can be designed by the engineer to fabricate a component with site specific material properties. During the FAST-DB process, diffusion bonding occurs, creating element concentration gradients across the discrete powder layers. The final product is a high density FAST-DB billet, including diffusion bonds with excellent integrity.

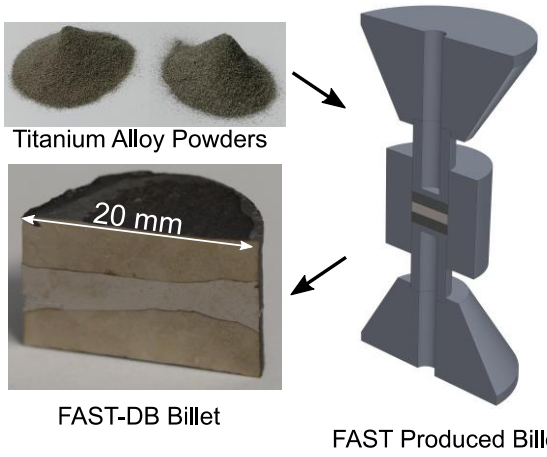

Fig. 1. A schematic illustration of the FAST-DB process - a novel solid-state approach of bonding dissimilar titanium alloy powders.

To demonstrate the bond complexity and detail that can be achieved in subcomponent regions of the FAST-DB process, a polymer 3D printed powder layup divider was used to produce a large-scale demonstrator slice of the term ‘FAST-DB’. The divider was put into an empty mould and the surrounding areas were filled with Ti-6-4 HDH powder, while CP-Ti HDH powder was used to fill the letters, shown in Fig. 2a. Prior to FAST processing, the divider was removed and the powder smoothed over, see Fig. 2b. Once consolidated, slices of the lettering were extracted and heat tinted to produce the demonstrator in Fig. 2c.

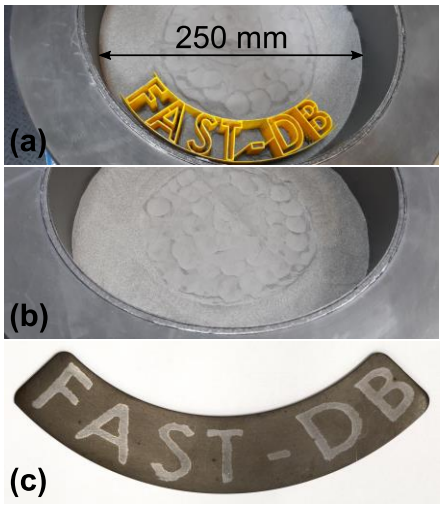

Fig. 2. (a) Photograph of a 3D printed polymer divider used to produce the 'FAST-DB' slice, in the FAST mould prior to the powder layup; **(b)** Photograph of the FAST powder layup after removal of the divider; **(c)** A slice of 'FAST-DB' processed on the large scale using CP-Ti HDH powder and the matrix as Ti-6-4 HDH powder. The sample was subsequently heat tinted to reveal the contrast between the two alloys.

In this paper the FAST-DB processing method is demonstrated as a new solid-state joining approach to diffusion bond dissimilar titanium alloy powders. The initial FAST-DB microstructures are analysed including hardness profiling, and diffusion profiles are established for a range of alloys.

2. Experimental Procedure

2.1 Materials

The three titanium alloy powders used; CP-Ti, Ti-6-4 and Ti-5553 were produced by gas atomisation and thus the powders are of a spherical morphology. The CP-Ti and Ti-6-4 powders were purchased from Arcam, while a Ti-5553 billet was atomised by TLS Technik Spezialpulver. Three bonds were analysed in this study consisting of Ti-5553 with CP-Ti, termed DB1, Ti-5553 with Ti-6-4, termed DB2, and Ti-6-4 with CP-Ti, termed DB3. The particle size distribution (PSD) was analysed using a Malvern Mastersizer 3000 laser particle size analyser with a wet dispersion method. A total of 20 measurements were obtained and an average taken for the Dx10, Dx50

and Dx90 statistical values. The distribution for CP-Ti and Ti-6-4 are nearly identical, while the Ti-5553 has a greater percentage of particles below 72.5 µm and a smaller percentage of particles above 72.5 µm compared to Ti-6-4, see Fig. 3. The Dx50 values for CP-Ti, Ti-6-4 and Ti-5553 are 71.1, 72.5 and 63.3, respectively.

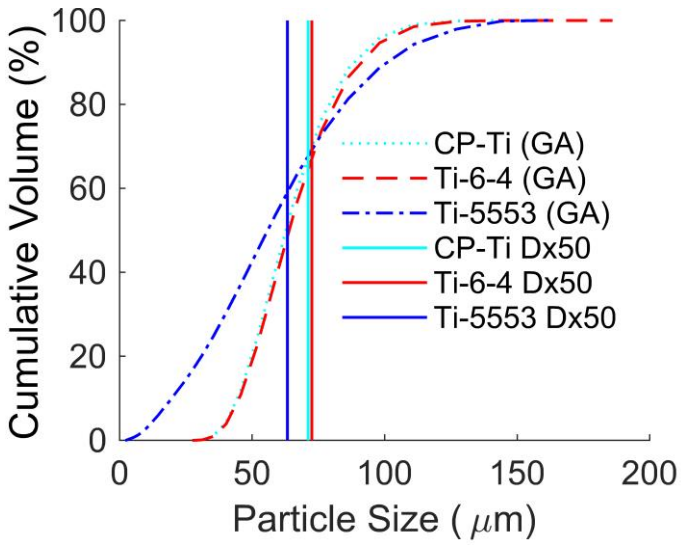

Fig. 3. Plot of cumulative volume against particle size including associated Dx50 values.

The chemistry of CP-Ti and Ti-6-4 powders were within ASTM B988-13 standards while the Ti-5553 chemistry was within 0.05% for Al, V and Mo, and within 0.1% for Cr compared to the designated chemistry. For each individual FAST-DB sample the alloy chemistries were measured using energy dispersive X-ray spectroscopy (X-EDS) analysis on a JEOL JSM-6490V SEM and a Philips XL-30 FEG.

The powders used to fabricate the large 250 mm FAST-DB billets were CP-Ti HDH and Ti-6-4 HDH, purchased from Phelly Materials Inc., NJ, USA in addition to the previously described Ti-5553 GA powder.

2.2 Experimental Approach

In the study, an FCT Systeme GmbH SPS Furnace Type HP D 25 with a vertical pyrometer for temperature control was used. The pyrometer measures the temperature 3 mm from the contact surface between the punch and powder for excellent control of the temperature during processing. The assembly consists of a 20 mm inner diameter graphite ring mould, punches and punch supports. The inner surface of the mould and the punch surfaces in contact with the powder were lined with graphite foil to eliminate powder bonding to the graphite mould, in addition to improving the ease of sample extraction. The mass of the powders used was based on producing a 15 mm deep theoretically fully consolidated sample. Once the powder mass had been measured, the powders were individually poured into the mould, producing a triple layer powder ‘sandwich’. No powder dividers were used in these small-scale samples. In all samples the Ti-5553 powder was sandwiched between either CP-Ti or Ti-6-4 alloy powders. Each powder charge was tapped to meet the tap density and flatten the powder layer, to produce the straightest diffusion bond possible on the macroscopic scale. To improve efficiencies by reducing heat loss through radiation from the assembly, a graphite felt jacket was wrapped around the mould. During processing the hydraulic rams applied pressure, while simultaneously applying a pulsed DC current through the assembly, providing the Joule heating to the powder.

The key FAST processing parameters for the small scale processing is summarised in Table 1. To reduce oxygen pickup at elevated temperatures, the processing chamber was filled with an inert argon atmosphere. Once the FAST dwell time was completed, the current was switched off allowing the sample to air cool to room temperature, and the load was returned to the starting force of 5 kN. The cooling rate was measured using the pyrometer and the data was analysed to determine an

average cooling rate. Once the sample had been removed, the graphite foil was removed using a grit blaster, followed by sectioning the sample in half perpendicular to the bond interface.

Table 1: Summary of the key FAST processing parameters used for small and large-scale processing.

	FAST Processing Parameter				
	Heating Rate (°C/min)	Pressure (MPa)	Dwell Temperature (°C)	Dwell Time (mins)	Cooling Rate (°C/min)
Small Scale	100	35	1200	10, 20, 60	240
Large Scale	25	35	1200	60	9

The tensile specimens were machined from 250 mm FAST billets produced at Kennametal UK Ltd., located in Newport, South Wales, UK, using a FCT Systeme GmbH SPS Furnace Type H-HP D 250. The key FAST parameters for the large-scale processing are summarised in Table 1. The powders were laid up with the bond interface parallel to the uniaxial compression force using 1 mm thick CP-Ti sheet dividers, which were manually removed. The tensile specimens were extracted using wire electrical discharge machining (EDM), then machine finished according to ASTM E8/E8M guidelines. The samples were tested to failure using a Tinius Olsen 25 ST benchtop tester with a constant crosshead speed of 0.01 mm s^{-1}. DB2 (Ti-5553 / Ti-6-4) and DB3 (Ti-6-4 / CP-Ti) samples were tested three times and the average UTS was calculated.

2.3 Analysis Techniques

To prepare the samples for analysis, standard metallographic procedures were used which included a final polishing stage incorporating 0.06 µm colloidal silica mixed with 30% concentration hydrogen peroxide. After hardness profiling, the samples were etched using Kroll's Reagent consisting of 2% HF, 6% HNO_3 and 92% H_2O for between 10 and 15 s, to reveal the alpha/beta morphology. The samples were viewed under a Reichert Jung Polyvar Met light microscope using cross-polarised light and an interference contrast lens to highlight relief. A FEI Inspect F50 SEM and FEI Talos F200X S/TEM were used to analyse the microstructure across the bond interface. The thin foils were prepared using focused ion beam (FIB) milling in a FEI Quanta 200 3D, prior to S/TEM analysis.

The hardness profiling was carried out using a Struers Durascan 70 G5 with automatic hardness evaluation. The method for analysing the hardness profile across the diffusion bond was dependent on the alloy combination as summarised in Table 2, however for all combinations a 15 s dwell time was used to adhere to the ASTM E384 standard.

Table 2: Summary of FAST-DB alloy combinations and the associated hardness profiling parameters used.

Bond	Alloy 1	Alloy 2	Microhardness Load (kgf)	Linear X-Distance Interval (µm)	Number of Indents
DB1	Ti-5553	CP-Ti	1.962	40	150
DB2	Ti-5553	Ti-6-4	9.81	50	100
DB3	Ti-6-4	CP-Ti	9.81	50	100

The hardness indents were imaged under light microscopy and ImageJ software by (Schneider et al., 2012) was used to measure the perpendicular distance from the bond line to the centre of the indent.

X-EDS point scans were used to measure element concentrations at locations across the diffusion bond. For all samples, the points were linearly spaced at 10 µm intervals to achieve good resolution for 10, 20, and 60 min dwell times, along a line perpendicular to the bond. Each point was analysed for 2 minutes to achieve the best accuracy, while not compromising the total time required for the point line scan. Three line scans consisting of individual points were used per sample, to ensure an accurate representation of diffusion was captured across the sample.

The length of the lines was dependent on the dwell time for the sample. Dwell times of 10, 20, and 60 mins required scan lengths of 300, 500 and 900 µm, respectively. As a key objective was to investigate elemental diffusion, the major and minor elements in the alloys; Ti, Al, V, Mo, Cr and Fe were analysed. Trace elements were disregarded in this study and the element concentrations were normalised.

MATLAB software (MATLAB 2018a) was used to determine the widths of the diffusion zones and the diffusion distance of individual elements into the parent materials. The curve fitting application was used to fit a curve to the three lines of raw X-EDS data. The start and finish points of the diffusion zone were determined by the interception locations at which the parent material element concentration lines cross the curve fit line, solved using simultaneous equations. An addition or subtraction of 0.01 wt.% to the average alloy element concentrations from Ti-5553 and Ti-6-4 was required to enable the lines to intercept, and for CP-Ti the element concentrations were set as 0.01 wt.% for all alloying elements.

2.4 Thermodynamic Modelling

Computational thermodynamic modelling of element diffusion across the diffusion bond was performed using DICTRA, the diffusion module within Thermo-Calc 2016a, as developed by (Andersson et al., 2002). It has already been proven to be successful in modelling the diffusion redistribution of alloying elements in titanium powder during sintering, as demonstrated by (Ivasishin et al., 2008). A one-dimensional diffusion couple system 1000 µm wide, with an interface directly in the middle, was setup for DB1 and DB2 using the titanium thermodynamic (TTTI3) and mobility databases (MOBTI) for dwell times of 10, 20, and 60 mins at 1200°C, excluding the heating and cooling regime. At this temperature, there are no phase changes due to the alloys being thermodynamically stable in the single beta phase, which reduces the complexity and computational time of the simulation.

3. Results and Discussion

3.1 Characteristic FAST-DB Microstructures

In DB1 (Fig. 4a) and DB2 (Fig. 4b) distinctive boundaries are prominent and are most easily observed using a topographical lens under light microscopy. As the FAST-DB bond is derived from powder, the interface has a natural irregular morphology at the micron scale. Importantly, in all bonded samples; no cracks, unbonded regions or voids were observed. Furthermore, there is no evidence of isolated particles in the parent material near to the bond interface, which suggests that no powder mixing occurs during FAST compression heating and cycle. A characteristic microstructural feature of dissimilar alloy bonds produced using the FAST-DB process, are grain boundaries that cross the diffusion bond interface and exist within both alloy microstructures, demonstrating that the bond has good

structural integrity, as shown in Fig. 4a, 4b and 4c. Interestingly, grains at the interface have a graded microchemistry, for example the grain highlighted in Fig. 4a has a Ti-5553 chemistry on the left hand side, moving to a CP-Ti chemistry on the right hand side. (He et al., 2012) observed similar behaviour when bonding Ti-6-4 sheets together using FAST, where grains and phases were observed to cross the bond interface.

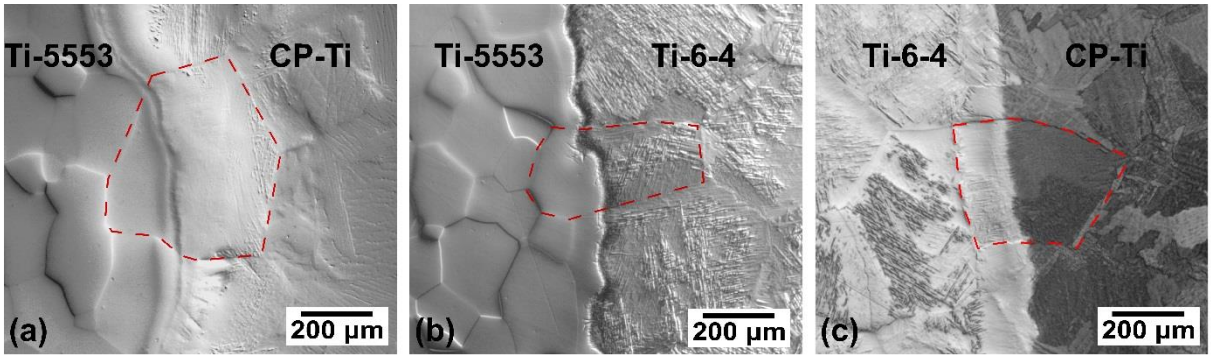

Fig. 4. **(a)** Grain boundary across DB1 interface between Ti-5553 and CP-Ti; **(b)** Grain boundary across DB2 interface between Ti-5553 and Ti-6-4; **(c)** Grain boundary across DB3 interface between Ti-6-4 and CP-Ti.

3.2 Microstructural Evolution and Hardness Profiles of FAST Diffusion Bonds

The microstructural evolution through DB1 (Ti-5553 / CP-Ti) is shown in Fig. 5a, and exhibits two distinct regions. The first is the Ti-5553 alloy on the left-hand side, which consists of large prior beta grains, and the CP-Ti alloy on the right.

From the corresponding hardness profile in Fig. 5d, the Ti-5553 alloy is harder than the CP-Ti alloy, as expected. The hardness profile has been divided into three distinct regions that are separate from the microstructural regions. In all DB1 samples, the first region shows a decrease in Ti-5553 hardness towards the interface. At the start of region 2, which is approximately 180 µm from the interface, the hardness increases rapidly to a peak hardness at the interface. To the right of the interface, the hardness of CP-Ti decreases at a similar rate, until the end of

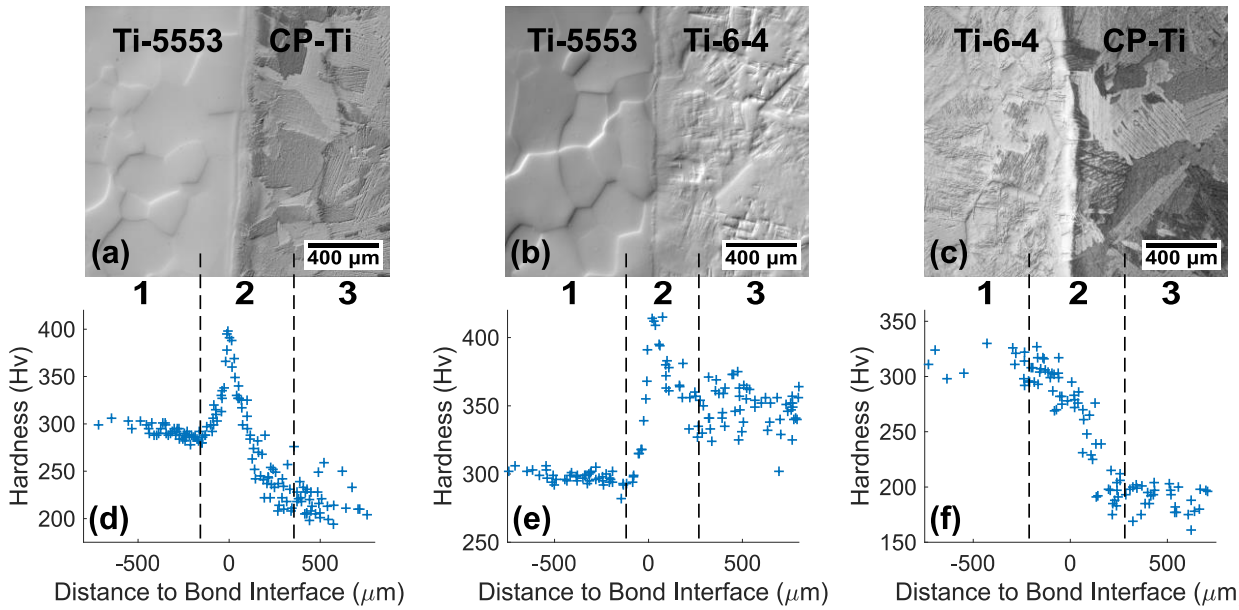

Fig. 5. (a,b,c) Light micrographs of FAST diffusion bonds between Ti-5553 with CP-Ti, Ti-5553 with Ti-6-4 and Ti-6-4 with CP-Ti; **(d,e,f)** Corresponding hardness profiles across DB1, DB2 and DB3.

region 2, located around 220 µm to the right of the diffusion bond interface. The third region displays a stabilisation of the hardness as the distance from the interface increases.

The microstructural evolution through DB2 (Ti-5553 / Ti-6-4) is shown in Fig. 5b, and exhibits two distinct regions. The Ti-5553 parent material on the left-hand side has the same large prior beta grains as seen in DB1, and on the right-hand side the Ti-6-4 parent material has a transformed alpha Widmanstätten microstructure.

The corresponding hardness profile of DB2 in Fig. 5e, shows that the Ti-5553 hardness decreases at a similar rate to the hardness behaviour in DB1. However, the start of region 2, where the hardness increases rapidly, is closer to the interface in DB2 compared to DB1, at approximately 85 µm. In region 2 the hardness increases up to a peak hardness which occurs within 50 µm into the Ti-6-4 material. From the interface to 220 µm to the right, the hardness decreases at a slower near linear rate. In region 3 the hardness levels out as the distance from the interface

increases. The Ti-6-4 microstructure contains both alpha and beta phases at room temperature, so there is a large deviation in hardness depending on where the hardness indentation is located. A higher indent load would reduce the deviation; however, it would also compromise the hardness profile resolution across the bond.

The microstructural evolution through DB3 (Ti-6-4 / CP-Ti) is shown in Fig. 5c, and exhibits two distinct regions. The Ti-6-4 parent material has the same microstructure in DB2, as seen in Fig. 5b, and the CP-Ti has the same microstructure in DB1, as seen in Fig. 5a.

The corresponding hardness profile of DB3 in Fig. 5f, shows that there is a smooth transition from the higher strength Ti-6-4 alloy into the lower strength CP-Ti alloy. In region 1, the hardness remains level until approximately 200 µm away from the bond interface, where the hardness gradually decreases across the diffusion bond, until around 280 µm to the right of the interface. In region 3 the hardness becomes level into the CP-Ti alloy.

A similar hardness profile trend is seen across DB1 and DB2 (Fig. 5d and Fig. 5e). Both show a spike in hardness within the diffusion bond, specifically at the interface in DB1 and within 50 µm in the Ti-6-4 alloy for DB2. This suggests that there is either a microstructural change from the parent material towards the interface or the formation of a higher strength phase or morphology.

Towards the bond interface, with an increase in beta stabilising chemistry, the alpha platelets become finer and their aspect ratio increases, resembling fine Widmanstätten morphology, as shown in Fig. 6a and Fig. 6c. The volume fraction of alpha laths decreases towards the interface and become progressively finer until they are no longer resolvable under SEM analysis. TEM samples were extracted by

FIB milling from the region associated with an increase in hardness, as highlighted by the red squares which represent the approximate location in Fig. 6a and Fig. 6c. In DB1 this was within 80 µm of the physical bond interface observed in Fig. 5d and in DB2 it was within 50 µm as shown Fig. 5e. The bright field STEM micrographs from DB1 and DB2 are shown in Fig. 6b and Fig. 6d, respectively. In both micrographs, fine scale alpha platelets in a martensitic matrix is observed. The fine scale alpha platelets have nucleated from the martensitic plates during cooling (at a rate of 4°C/s) from 1200°C. These fine scale alpha platelets have created a high number of alpha/beta interfaces that act as dislocation barriers, thus locally increasing the strength in the bond region, as shown by (Deurig and Williams, 1983). In Fig. 6b there is a lower lath aspect ratio ranging from 28 to 152 nm wide, and in Fig. 6d a finer alpha lath size and smaller range is observed with widths from 8 to 40 nm. The FAST-DB process could be used as a method to engineer desired microstructures with specific phase morphologies and the related mechanical properties.

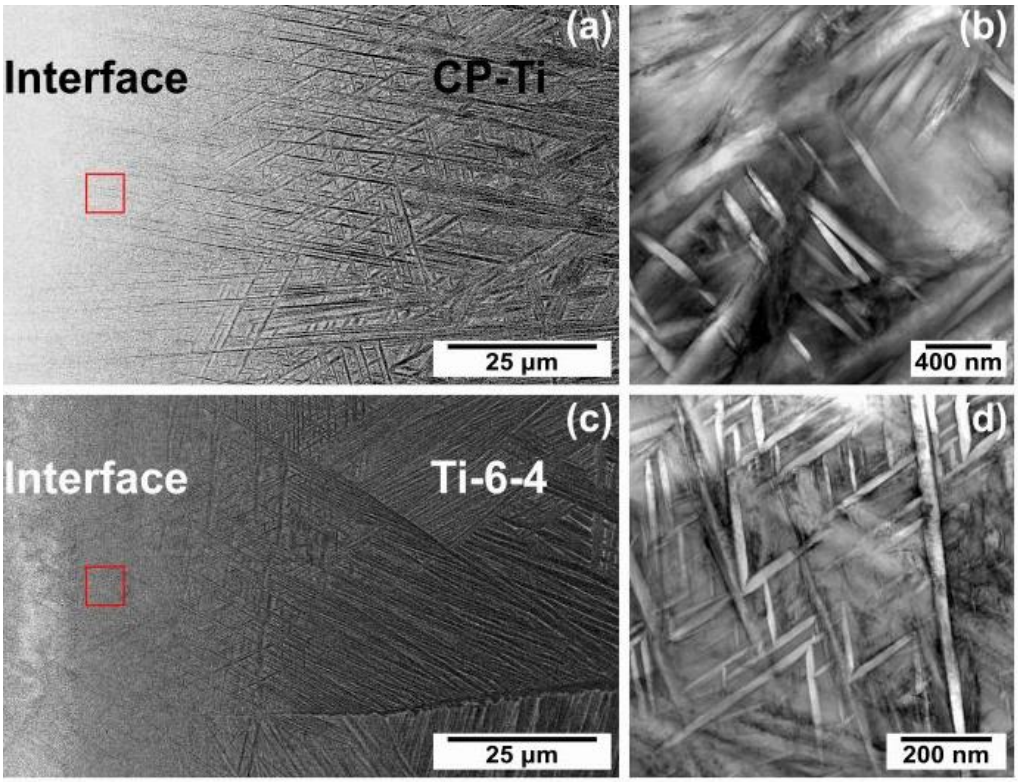

Fig. 6. (a) BSE image of the microstructural change near to the interface of DB1. The red box indicates the approximate TEM sample extraction location; **(b)** STEM image showing fine scale alpha near to the DB1 interface; **(c)** BSE image of the microstructural change near to the interface of DB2. The red box indicates the approximate TEM sample extraction location; **(d)** STEM image showing fine scale alpha near to the DB2 interface.

The effects of changing individual element chemistry in the Ti-Mo_x system was investigated by (Collins et al., 2003) and the Ti-V_x system by (Banerjee et al., 2003) using a feedstock process with high cooling rates. As the V content increased from 3 to 5 at.%, and Mo content from 1 to 2.2 at.%, the beta phase volume increased and the average alpha lath width decreased with an accompanying increase in hardness.

3.3 Measured and Predicted Elemental Profiles across FAST-DB Interfaces

In DB1 and DB2, the elemental distribution measured by X-EDS gradually changes across the FAST diffusion bond interface from one alloy into the other. The change in elemental distribution can be curve fitted using the complimentary error function in Equation 1,

$$c = \frac{A_0}{2} erfc\left(\frac{x - J1}{2\sqrt{J2}}\right) \quad (1)$$

where c is the element concentration at a given distance, A_0 is the initial element concentration before diffusion occurs, $erfc$ is the complimentary error function and x is the perpendicular distance from the bond interface measured in microns. $J1$ and $J2$ are coefficients that are calculated by MATLAB. This is in agreement with the solution by (Crank, 1955) of an example problem where two metallic bars are in contact with each other end to end with an arbitrary dwell time, which assumes the materials form an ideal solution and the diffusion coefficient is constant.

Fig. 7 and Fig. 8 shows the complimentary error function curve fit for the elements of Al, V, Mo and Cr for DB1 and DB2. For a dwell time of 60 mins in DB1, the total solid solution zone width is approximately 525 µm, which is similar to that observed in DB2 where the width is 555 µm. Furthermore, the diffusion distances calculated for all elements in both DB1 and DB2 were comparable. Both solid solution zones are larger than the average grain size produced, demonstrating that elemental diffusion has occurred across prior powder particle boundaries, as shown in Fig. 5a and Fig. 5b.

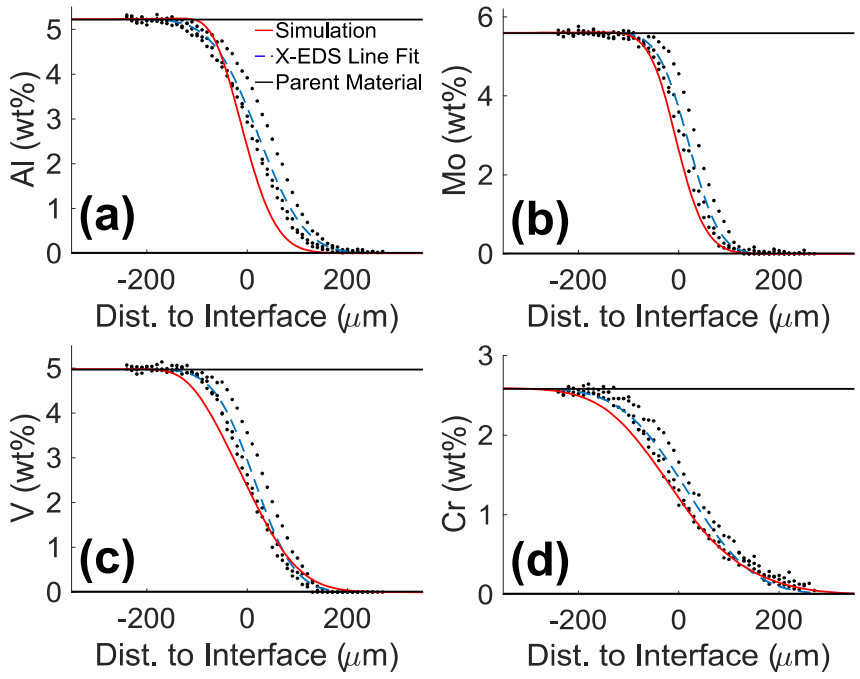

Fig. 7. Plots showing the change in element concentration measured from X-EDS, across the Ti-5553 with CP-Ti (DB1) FAST-DB interface after a 60 min dwell time; **(a)** Al; **(b)** Mo; **(c)** V; **(d)** Cr.

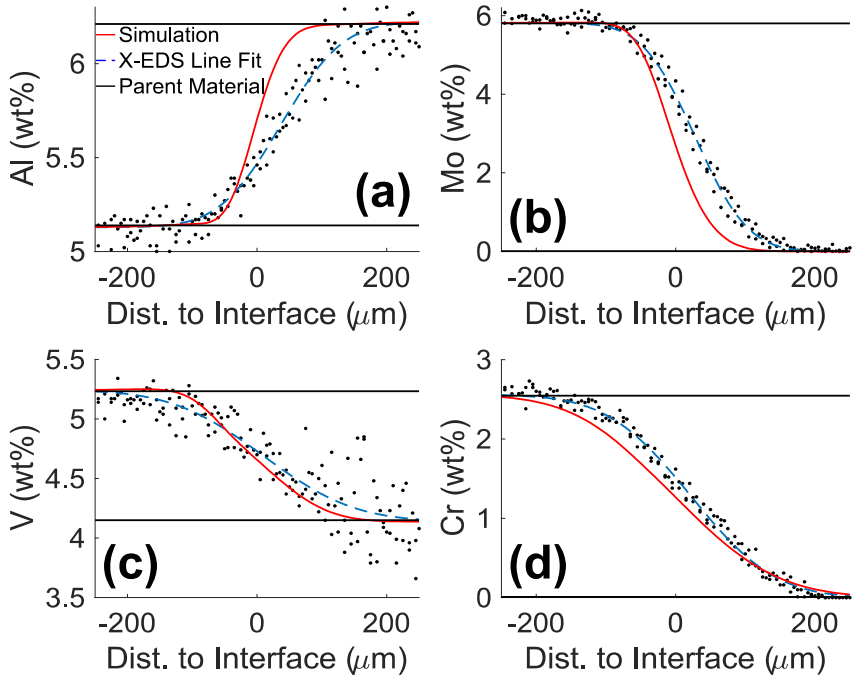

Fig. 8. Plots showing the change in element concentration across the Ti-5553 with Ti-6-4 (DB2) FAST-DB interface after a 60 min dwell time. **(a)** Al; **(b)** Mo; **(c)** V; **(d)** Cr.

The thermodynamic modelling predictions of element concentration across the bond are in close agreement with the X-EDS data, as shown in Fig. 7 and Fig. 8. For Al and Mo there is a slight underestimation of the diffusion profile in both DB1 and DB2 samples, while Cr has a slight overestimation. On the other hand, V is slightly overestimated in DB1 and underestimated in DB2, although it has the closest prediction of the diffusion profile out of all the alloying elements.

The diffusion kinetics model of FAST processing provides good approximations of the diffusion distances expected in DB1 and DB2 samples. DICTRA is limited to modelling ideal systems and does not include microstructural considerations such as percentage volume, phase morphology, area percentage of grain boundaries or porosity, which will affect the diffusion kinetics of the alloying elements.

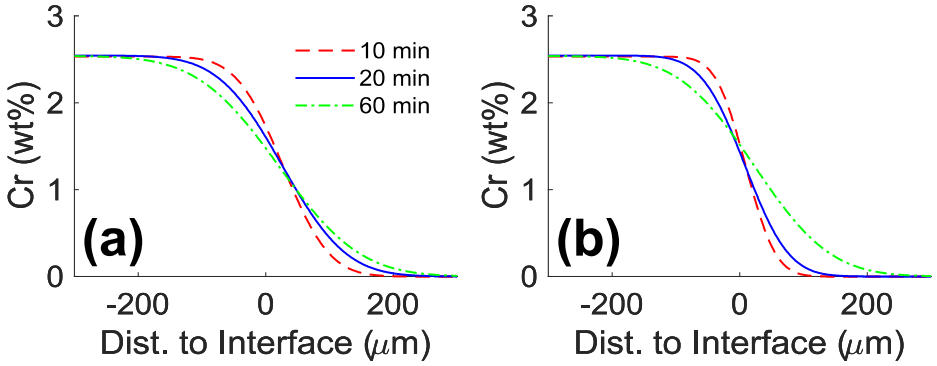

Fig. 9. (a) Plot showing the X-EDS diffusion profile for the chromium concentration change across DB1 at different dwell times; **(b)** Plot showing the X-EDS diffusion profile for chromium concentration change across DB2 at different dwell times.

As the dwell time increases, the gradient of the diffusion profile becomes shallower indicating that the elements are diffusing deeper into the respective alloys. This is demonstrated through the X-EDS diffusion profile line fit for chromium at different

dwell times for DB1 and DB2 in Fig. 9a and Fig. 9b, respectively. At the bond interface, the chromium element concentration is similar for DB1 and DB2 samples.

3.4 FAST-DB Diffusion Kinetics

To determine the relationship between the diffusion zone sizes and the dwell time, the diffusion distance was plotted against $1/\sqrt{\tau}$ where τ is the dwell time. In DB1 (Ti-5553 / CP-Ti), a clear linear relationship was found for all elements at 10, 20, and 60 min dwell times as shown in Fig. 10. Additionally, the linear best fit line for Cr has the steepest gradient followed by Al, V and Mo, in both Ti-5553 and CP-Ti alloys.

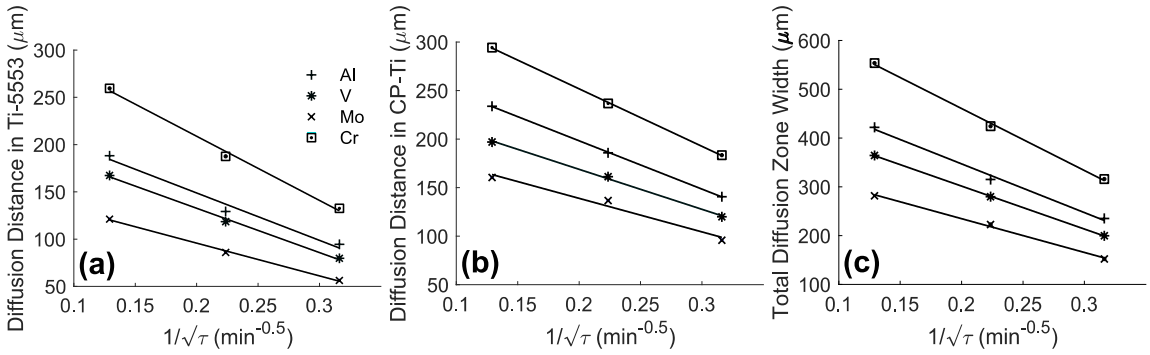

Fig. 10. DB1. **(a)** Plot of diffusion distance in Ti-5553 against dwell time; **(b)** Plot of diffusion distance in CP-Ti against dwell time; **(c)** Plot of total diffusion zone width against dwell time.

As expected, a longer dwell time at 1200°C leads to a greater diffusion distance into the CP-Ti, and in the Ti-5553 alloy. Elemental diffusion in the Ti-5553 and CP-Ti alloy, and overall diffusion zone width is ordered as Cr being the fastest diffuser, followed by Al, V and Mo. Diffusion coefficient data consisting of pure titanium and a pure element has been collated by (Pereloma et al., 2012) and compared at temperatures ranging from 600 to 1600°C. At 1200°C, in beta-Ti the diffusion coefficients were reported graphically as Cr being the fastest, followed by V, Al and

Mo which is almost identical to the diffusion kinetics occurring in DB1, except Al and V being reversed. This suggests the diffusion kinetics during FAST processing are similar to conventional solid-state bonding, despite the comparative complexity of the system to simple diffusion couples. To compare the alloying elements against each other the driving force for chemical homogenisation must be considered. Al, V and Mo all have a chemical difference of 5 wt.% so the driving force is equal, however Cr only has a difference of 3 wt.%. Even with a reduced driving force, Cr has still been shown to diffuse the quickest.

3.5 Tensile Testing

Fig. 11a and Fig. 11b shows a typical fractured tensile test for DB2 and DB3, respectively. In DB2, the average UTS was 923 ± 81 MPa while the average UTS for DB3 was 474 ± 36 MPa. In all but one tensile test, the failure occurred in the lower strength alloy, demonstrating the bond consistently has good structural integrity. Furthermore, it proves that the fine scale alpha with martensitic matrix at the bond interface, as shown in Fig. 6b and 6d, is not detrimental to the tensile properties. Instead, the small size of the incoherent alpha platelets causes them to be resistant to plastic deformation and consequently generates high yield strength in the region.

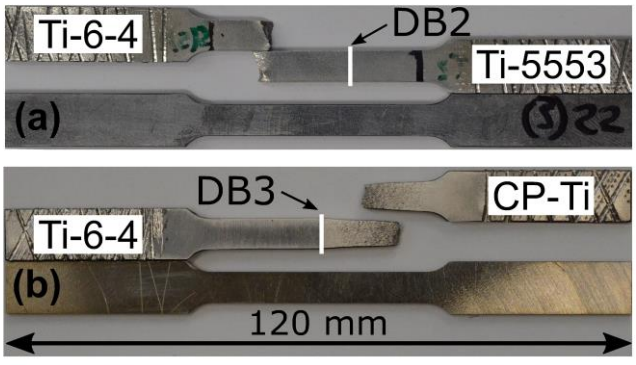

Fig. 11. Tensile specimens of **(a)** DB2 (Ti-5553 with Ti-6-4); **(b)** DB3 (Ti-6-4 with CP-Ti).

6. Conclusions

FAST-DB is a novel approach of diffusion bonding dissimilar titanium powder alloys, specifically Ti-5553 with CP-Ti, Ti-5553 with Ti-6-4 and Ti-6-4 with CP-Ti. All bonds exhibited excellent mechanical integrity, as a result of smooth elemental diffusion profiles across the bond interface, which can be reliably predicted using commercial thermodynamic software. As a demonstration during tensile testing neither DB2 nor DB3 failed, as failure occurred in the lower strength alloy. In bonds containing Ti-5553, processing conditions were such that fine scale alpha can be generated at the bond interface, underlined by high hardness values. Yet, such features were not detrimental to the bond mechanical response, and instead architectured a high strength region. Consequently, FAST-DB of dissimilar titanium alloy compositions could be a novel solid-state technique to engineer specific fine scale alpha morphologies.

In the short term, prototype aerospace and automotive dynamically loaded components, up to approximately 300 mm diameter, will be manufactured and tested. In the longer term, FAST-DB will provide designers and engineers a new approach to manufacturing components that will benefit from dissimilar alloys in different subcomponent regions.

Acknowledgements

The authors acknowledge the Engineering and Physical Sciences Research Council's Advanced Metallic Systems Centre for Doctoral Training for funding J. J. Pope (Grant Number EP/G036950/1). The authors also acknowledge Dr Adam

Tudball from Kennametal Ltd. UK for help with processing the large FAST-DB billets, Michael Kenyon from the University of Manchester for STEM usage and operation, and finally Metalysis Ltd. for the use of their SEM for X-EDS analysis.

References

Andersson, J.O., Helander, T., Höglund, L., Shi, P., Sundman, B., 2002. THERMO-CALC & DICTRA, Computational Tools For Materials Science. Calphad 26, 273–312. doi:https://doi.org/10.1016/S0364-5916(02)00037-8

Banerjee, R., Collins, P.C., Bhattacharyya, D., Banerjee, S., Fraser, H.L., 2003. Microstructural evolution in laser deposited compositionally graded α/β titanium - vanadium alloys. Acta Mater. 51, 3277–3292. doi:https://doi.org/10.1016/S1359-6454(03)00158-7

Boyer, R.R., Briggs, R.D., 2005. The Use of β Titanium Alloys in the Aerospace Industry. J. Mater. Eng. Perform. 14, 681–685. doi:https://doi.org/10.1361/105994905X75448

Calvert, E., Wynne, B., Weston, N., Tudball, A., Jackson, M., 2018. Thermomechanical processing of a high strength metastable beta titanium alloy powder, consolidated using the low-cost FAST- forge process. J. Mater. Process. Technol. 254, 158–170. doi:10.1016/j.jmatprotec.2017.11.035

Chen, H., Luo, L., Zhang, J., Zan, X., Zhu, X., 2015. Investigation on W / Fe diffusion bonding using Ti foil and Ti powder interlayer by SPS. J. Nucl. Mater. 467, 566–571. doi:10.1016/j.jnucmat.2015.10.045

Collins, P.C., Banerjee, R., Banerjee, S., Fraser, H.L., 2003. Laser deposition of compositionally graded titanium - vanadium and titanium - molybdenum alloys.

Mater. Sci. Eng. A 352, 118–128. doi:https://doi.org/10.1016/S0921-5093(02)00909-7

Crank, J., 1955. Methods of solution when the diffusion coefficient is constant, in: Mathematics of Diffusion. pp. 11–14.

Deurig, T.W., Williams, J.C., 1983. Overview: microstructure and properties of beta titanium alloys. Beta Titan. Alloy. 1980's 19–67.

Dong, P., Wang, Z., Wang, W., Chen, S., Zhou, J., 2016. Understanding the spark plasma sintering from the view of materials joining. Scr. Mater. 123, 118–121. doi:10.1016/j.scriptamat.2016.06.014

Gangwar, K., Ramulu, M., Cantrell, A., Sanders, D.G., 2016. Microstructure and Mechanical Properties of Friction Stir Welded Dissimilar Titanium Alloys: TIMET-54M and ATI-425. Metals (Basel). 6, 252. doi:https://doi.org/10.3390/met6100252

Gudipati, P.P., Kosaka, Y., 2016. Diffusion bonding of similar and dissimilar titanium alloys, in: Proceedings of the 13th World Conference on Titanium. pp. 1631–1636.

He, D., Fu, Z., Wang, W., Zhang, J., Munir, Z.A., Liu, P., 2012. Temperature-gradient joining of Ti – 6Al – 4V alloys by pulsed electric current sintering. Mater. Sci. Eng. A 535, 182–188. doi:https://doi.org/10.1016/j.msea.2011.12.061

Ivasishin, O.M., Eylon, D., Bondarchuk, V.I., Savvakin, D.G., 2008. Diffusion during Powder Metallurgy Synthesis of Titanium Alloys. Defect Diffus. Forum 277, 177–185. doi:https://doi.org/10.4028/www.scientific.net/DDF.277.177

Ji, Y., Wu, S., Zhao, D., 2016. Microstructure and Mechanical Properties of Friction

Welding Joints with Dissimilar Titanium Alloys. Metals (Basel). 6, 108. doi:https://doi.org/10.3390/met6050108

Lütjering, G., Williams, J.C., 2007. Titanium : Engineering Materials and Processes. doi:https://doi.org/10.1007/978-3-540-73036-1

Martin, G., Fabrègue, D., Mercier, F., Chafino-Aixa, J.A., Dendievel, R., Blandin, J.J., 2016. Coupling electron beam melting and spark plasma sintering: A new processing route for achieving titanium architectured microstructures. Scr. Mater. 122, 5–9. doi:10.1016/j.scriptamat.2016.05.001

MATLAB 2018a, MATLAB 2016b, The Mathworks, Inc., Natick, Massachussets, United States.

Miriyev, A., Stern, A., Tuval, E., Kalabukhov, S., Hooper, Z., Frage, N., 2013. Titanium to steel joining by spark plasma sintering (SPS) technology. J. Mater. Process. Technol. 213, 161–166. doi:https://doi.org/10.1016/j.jmatprotec.2012.09.017

Pereloma, E., Savvakin, D., Carman, A., Gazder, A., Ivasishin, O., 2012. Microstructure development and alloying elements diffusion during sintering of near-beta titanium alloys. Key Eng. Mater. 520, 49–56. doi:https://doi.org/10.4028/www.scientific.net/KEM.520.49

Pripanapong, P., Umeda, J., Imai, H., Takahashi, M., Kondoh, K., 2016. Tensile Strength of Ti/Mg Alloys Dissimilar Bonding Material Fabricated by Spark Plasma Sintering. Int. J. Eng. Innov. Res. 5, 253–259.

Schneider, C.A., Rasband, W.S., Eliceiri, K.W., 2012. NIH Image to ImageJ: 25 years of image analysis. Nat Meth 9, 671–675.

Shahedi, M.S., Namini, A.S., Motallebzadeh, A., Azadbeh, M., 2018. Effects of sintering temperature on microstructure and mechanical properties of spark plasma sintered titanium. Mater. Chem. Phys. 203, 266–273. doi:10.1016/j.matchemphys.2017.09.069

Suárez, M., Fernández, A., Menéndez, J.L., Torrecillas, R., Kessel, H.U., Hennicke, J., Kirchner, R., Kessel, T., 2013. Challenges and Opportunities for Spark Plasma Sintering : A Key Technology for a New Generation of Materials, in: Sintering Applications. pp. 319–342. doi:https://doi.org/10.5772/53706

Vicente, N., Fedrizzi, A., Bazzanella, N., Casari, F., Buccioti, F., Molinari, A., 2013. Microstructure of interface of SPS co-sintered and sinter bonded cp2-Ti and Co – 28Cr – 6Mo. Powder Metall. 56, 143–148. doi:http://dx.doi.org/10.1179/1743290112Y.0000000040

Weston, N.S., Derguti, F., Tudball, A., Jackson, M., 2015. Spark plasma sintering of commercial and development titanium alloy powders. J. Mater. Sci. 50, 4860–4878. doi:https://doi.org/10.1007/s10853-015-9029-6

Zhao, K., Liu, Y., Huang, L., Liu, B., He, Y., 2016. Diffusion bonding of Ti-45Al-7Nb-0.3W alloy by spark plasma sintering. J. Mater. Process. Technol. 230, 272–279. doi:https://doi.org/10.1016/j.jmatprotec.2015.11.030